BIOCHEMISTRY
including biophysical chemistry & molecular biology

ARTICLE

pubs.acs.org/biochemistry

Structures of β-Hairpin Antimicrobial Protegrin Peptides in Lipopolysaccharide Membranes: Mechanism of Gram Selectivity Obtained from Solid-State Nuclear Magnetic Resonance

Yongchao Su,[†] Alan J. Waring,[‡,§] Piotr Ruchala,[‡] and Mei Hong*[,†]

[†]Department of Chemistry, Iowa State University, Ames, Iowa 50011, United States

[‡]Department of Medicine, David Geffen School of Medicine, University of California, Los Angeles, California 90095, United States

[§]Department of Physiology and Biophysics, School of Medicine, University of California, Irvine, California 92697-4560, United States

Supporting Information

ABSTRACT: The structural basis for the Gram selectivity of two disulfide-bonded β-hairpin antimicrobial peptides (AMPs) is investigated using solid-state nuclear magnetic resonance (NMR) spectroscopy. The hexa-arginine PG-1 exhibits potent activities against both Gram-positive and Gram-negative bacteria, while a mutant of PG-1 with only three cationic residues maintains Gram-positive activity but is 30-fold less active against Gram-negative bacteria. We determined the topological structure and lipid interactions of these two peptides in a lipopolysaccharide (LPS)-rich membrane that mimics the outer membrane of Gram-negative bacteria and in the POPE/POPG membrane, which mimics the membrane of Gram-positive bacteria. ^{31}P NMR line shapes indicate that both peptides cause less orientational disorder in the LPS-rich membrane than in the POPE/POPG membrane. ^{13}C chemical shifts and ^{13}C−^{1}H dipolar couplings show that both peptides maintain their β-hairpin conformation in these membranes and are largely immobilized, but the mutant exhibits noticeable intermediate-time scale motion in the LPS membrane at physiological temperature, suggesting shallow insertion. Indeed, ^{1}H spin diffusion from lipid chains to the peptides shows that PG-1 fully inserts into the LPS-rich membrane whereas the mutant does not. The ^{13}C−^{31}P distances between the most hydrophobically embedded Arg of PG-1 and the lipid ^{31}P are significantly longer in the LPS membrane than in the POPE/POPG membrane, indicating that PG-1 does not cause toroidal pore defects in the LPS membrane, in contrast to its behavior in the POPE/POPG membrane. Taken together, these data indicate that PG-1 causes transmembrane pores of the barrel-stave type in the LPS membrane, thus allowing further translocation of the peptide into the inner membrane of Gram-negative bacteria to kill the cells. In comparison, the less cationic mutant cannot fully cross the LPS membrane because of weaker electrostatic attractions, thus causing weaker antimicrobial activities. Therefore, strong electrostatic attraction between the peptide and the membrane surface, ensured by having a sufficient number of Arg residues, is essential for potent antimicrobial activities against Gram-negative bacteria. The data provide a rational basis for controlling Gram selectivity of AMPs by adjusting the charge densities.

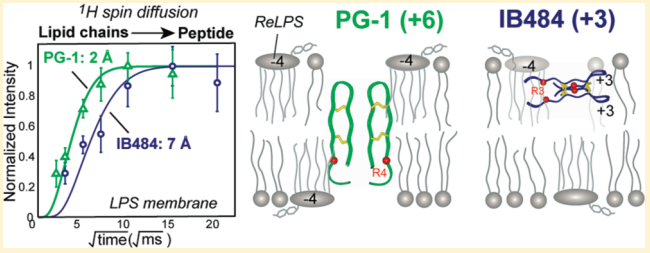

As a consequence of evolution, a large number of bacterial strains have developed resistance to conventional antibiotics, making the design of new antimicrobial molecules an urgent need.[1,2] Antimicrobial peptides (AMPs), small cationic peptides of the innate immune systems of many animals and plants, have attracted much attention as potential antibiotics because of their potent and broad-spectrum activities.[3,4] The mechanisms of action of AMPs have been extensively investigated using biophysical and biochemical methods.[5−8] These studies showed that a large number of AMPs kill bacteria by disrupting the membrane integrity[6] or altering the membrane potential[9,10] of the microbial cells. Thus, the structures of the protective layers of bacterial cells traversed and disrupted by AMPs are relevant for understanding AMP's mechanisms of action. Gram-positive bacteria are coated with a thick peptidoglycan layer that is several tens of nanometers thick and an inner phospholipid bilayer, while Gram-negative bacteria are protected by a lipopolysaccharide (LPS)-rich outer membrane, a thin periplasmic peptidoglycan layer, and an inner phospholipid bilayer (Figure 1).[11] The outer membrane of Gram-negative bacteria is compositionally asymmetric: LPS molecules cover ∼90% of the outer membrane surface, while phospholipids compose the inner leaflet.[12] It is known that the activity of many AMPs that target Gram-negative bacteria is concurrent upon permeabilization of the inner phospholipid bilayer rather than the outer membrane. This is true, for example, for the β-sheet-rich and disulfide-bonded protegrin-1 (PG-1) and human β-defensins.[9,13] Thus, these AMPs must first bind to and cross the LPS-rich outer membrane before reaching their target phospholipid bilayer. As a corollary, AMPs that are active against Gram-positive bacteria but not Gram-negative

Received: December 12, 2010
Revised: February 7, 2011
Published: February 08, 2011

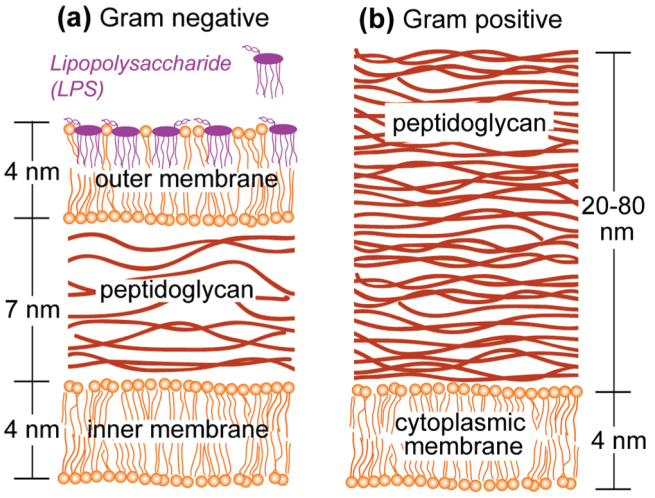

Figure 1. Schematics of the different membrane structure of bacteria. (a) Gram-negative bacteria have a lipopolysaccharide (LPS)-rich outer membrane, a thin peptidoglycan layer, and an inner phospholipid membrane. (b) Gram-positive bacteria have a thick peptidoglycan layer and a cytoplasmic membrane. The main phospholipids in both bacteria are phosphatidylethanolamine (PE) and phosphatidylglycerol (PG).[79] LPS is ~10 mol % of the phospholipid amount in *Escherichia coli* cells.[38] The long O-antigen chain of LPS is shortened for the sake of simplicity.

bacteria must be discriminated by the LPS membrane. Therefore, elucidating the structure and lipid interactions of AMPs in the LPS-rich membrane is important for understanding the mechanism of Gram selectivity.

LPS is a negatively charged complex glycolipid that can be divided into three structural regions: the hydrophobic lipid A that anchors LPS to the membrane, an oligosaccharide core, and an O-antigen polysaccharide.[11,14] The lipid A moiety consists of four to seven acyl chains attached to a diglucosamine diphosphate and is responsible for the severe host inflammatory responses triggered by LPS.[11,15] The oligosaccharide core can be divided into the inner core, which contains a Kdo (3-deoxy-D-*manno*-oct-2-ulosonic acid) disaccharide and heptoses, and a structurally diverse outer core. The LPS derived from the *Escherichia coli* deep rough mutant, ReLPS (Figure 2b), contains only lipid A and two Kdo units yet retains most of the endotoxin activity of native LPS.[16] This structurally homogeneous ReLPS is thus an appealing molecule for investigating AMP−LPS interactions.

A number of biophysical and biochemical studies have probed the interactions of AMPs with LPS.[14,17−22] Most of these studies indicate that strong binding of AMPs to LPS is necessary for potent antimicrobial activity. For example, transmission electron and atomic force microscopies were used to study the effects of NK-lysin peptides on the morphology of different Gram-negative bacteria. The results suggested that electrostatic interaction with LPS was the decisive factor that correlated with bacterial killing,[18] while subsequent outer membrane intercalation and permeabilization are mostly independent of the chemical structure of the LPS oligosaccharides. Several solution nuclear magnetic resonance (NMR) studies gave high-resolution structures of AMPs bound to LPS micelles and showed favorable electrostatic interactions between the cationic residues of the peptides and the anionic phosphates and Kdo units of LPS.[14,17] However, the biochemical studies used vesicles or real cells and had a low structural resolution, while high-resolution solution NMR

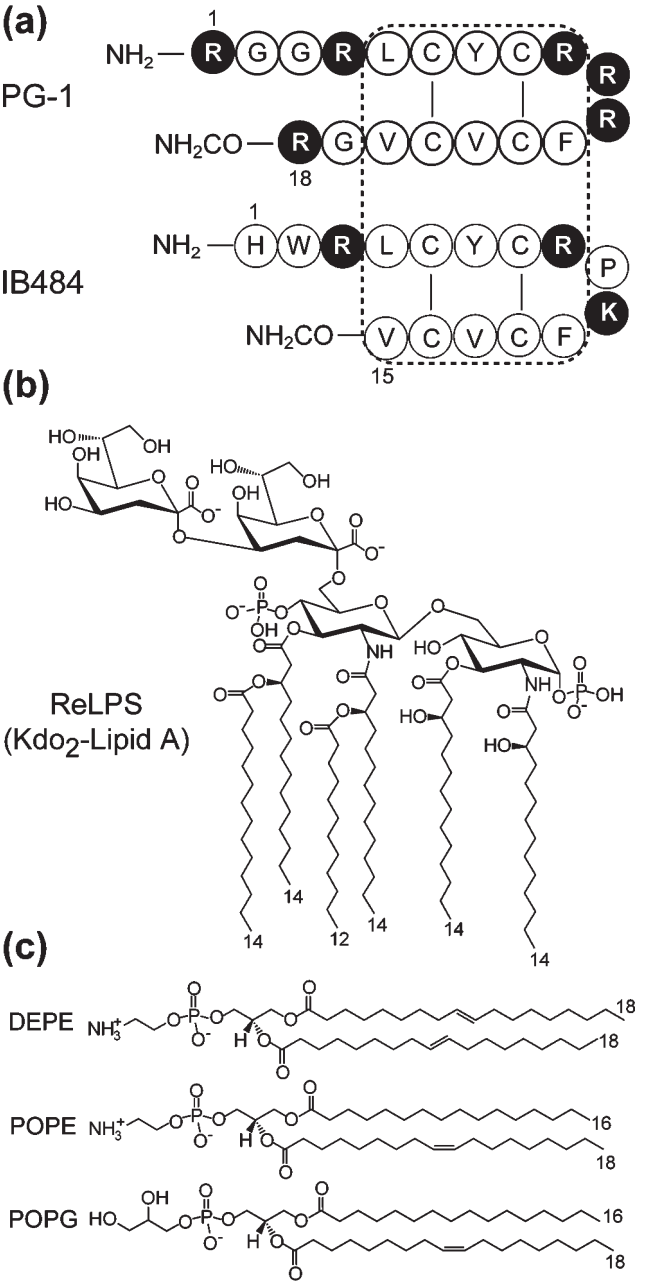

Figure 2. Chemical structures of the peptides and lipids used in this study. (a) Amino acid sequences of disulfide-bonded PG-1 and IB-484. (b) Chemical structure of ReLPS. (c) Chemical structures of DEPE, POPE, and POPG.

studies used LPS micelles or monolayers, which do not represent the bilayer nature of outer membranes well.

Here, we investigate two protegrin peptides, PG-1 and a charge-reduced mutant, IB484, to understand the structural basis underlying the Gram selectivity of β-hairpin AMPs. PG-1 is a porcine-derived 18-residue disulfide-bonded AMP containing six Arg residues (Figure 2a). It is active against both Gram-positive and Gram-negative bacteria, with minimal inhibitory concentrations (MICs) of 0.3−3.0 μM.[23,24] The mutant IB484 contains the same disulfide bonds but only three cationic residues, two Arg residues and one Lys (Figure 2a). Its activity against Gram-positive methicillin-resistant *Staphylococcus aureus* (MRSA) is comparable to that of PG-1, but its activity against Gram-negative

Table 1. Minimal Inhibitory Concentrations (MICs) of PG-1 and IB484 against Two Types of Bacteria[a]

peptide	MRSA (Gram-positive)	*P. aeruginosa* (Gram-negative)
PG-1	1	1
IB484	2	32

[a] The MIC values were normalized to those of PG-1, which are 1-4 μg/mL against MRSA and 0.2-2 μg/mL against *P. aeruginosa*. The data were taken from ref 25.

Pseudomonas aeruginosa is more than 30-fold weaker than that of PG-1.[25] The MIC values of PG-1 and IB484 are listed in Table 1. Our previous solid-state NMR studies showed that PG-1 disrupts anionic POPE/POPG membranes by forming transmembrane (TM) oligomeric β-barrels. Some of the lipid molecules around these β-barrels embed their phosphate groups into the hydrophobic middle of the membrane, thus connecting the two membrane leaflets.[6,26−33] The formation of these toroidal pores explains the antimicrobial activity of PG-1 against Gram-positive bacteria. However, how PG-1 interacts with the LPS membrane of Gram-negative bacteria has not been studied. Further, the topological structures of the Gram-selective IB484 in the two types of lipid membranes are completely unknown.

In this study, we use solid-state NMR spectroscopy to determine the structure and lipid interaction of PG-1 and IB484 in lipid membranes that mimic the Gram-positive and Gram-negative bacterial cell surfaces. ^{31}P NMR was used to examine the nature and extent of membrane disorder caused by these peptides. The peptide conformation and dynamics were characterized by two-dimensional (2D) ^{13}C−^{13}C correlation and dipolar-chemical-shift (DIPSHIFT) correlation experiments. We then determined the depth of insertion of PG-1 and IB484 in the two types of membranes using ^{1}H spin diffusion and ^{13}C−^{31}P distance measurements. From the observed structural differences, we propose mechanistic models for the Gram selectivity of the charge-reduced mutant as well as the interaction of wild-type PG-1 with the LPS membrane of Gram-negative bacteria.

MATERIALS AND METHODS

Lipids and Peptides. All lipids, including 1-palmitoyl-2-oleoyl-*sn*-glycero-3-phosphoethanolamine (POPE), 1-palmitoyl-2-oleoyl-*sn*-glycero-3-phosphatidylglycerol (POPG), 1,2-dielaidoyl-*sn*-glycero-3-phosphoethanolamine (DEPE) (Figure 2c), and the deep rough mutant ReLPS isolated from *E. Coli* strain WBB06, were purchased from Avanti Polar Lipids (Alabaster, AL). ReLPS (Kdo_2-Lipid A) has endotoxin activity comparable to that of native LPS and can now be obtained at high purity on a large scale.[34] Fmoc-protected ^{13}C- and ^{15}N-labeled Val was prepared in-house, while backbone- and side chain-protected ^{13}C- and ^{15}N-labeled Arg was purchased from Cambridge Isotope Laboratories.

PG-1 (RGGRLCYCRRRFCVCVGR-$CONH_2$) and IB484 (HWRLCYCRPKFCVCV-$CONH_2$) were synthesized using Fmoc solid-phase synthesis protocols and purified by reversed-phase HPLC. The peptides were oxidized and folded as described previously[29] to yield the correct disulfide linkages. The disulfide connectivity pattern is the same between synthetic and natural protegrin peptides based on sequential enzyme digestion combined with mass spectrometry analysis[35] and solution NMR studies.[36,37] The PG-1 sample contained labeled Arg4, while the IB484 sample contained labeled Arg3 and Val13.

Membrane Sample Preparation. POPE and POPG were mixed at a 3:1 molar ratio in chloroform, dried under nitrogen gas, redissolved in cyclohexane, and lyophilized overnight. The homogeneous dry powder was suspended in 2 mL of phosphate buffer (10 mM, pH 7.0) and frozen and thawed six times to yield a transluscent vesicle solution. Approximately 5.5 mg of peptide was dissolved in 0.5 mL of phosphate buffer. The lipid vesicle solution was added to the peptide solution, which immediately caused precipitation, indicating membrane binding of the peptides. The solution was incubated overnight at 4 °C, followed by ultracentrifugation at 55000 rpm and 6 °C for 3 h to yield a membrane pellet. UV−vis analysis indicated >95% binding of the peptide to the membrane. The water content of the pellet was adjusted to 40% (w/w) by slow evaporation of the samples in a desiccator. The pellet was center-packed into a 4 mm NMR rotor.

The LPS membrane contained ReLPS and DEPE at a 1:5 molar ratio (~3:5 mass ratio) to mimic the outer membrane composition of Gram-negative bacteria.[38] The two lipids were codissolved in a chloroform/methanol mixture (4:1, v/v) and subjected to the same procedure as described above to produce the proteoliposomes. All peptide-containing membranes had a peptide:lipid molar ratio of 1:12.5.

Solid-State NMR Spectroscopy. NMR experiments were conducted on a 9.4 T wide-bore Bruker (Karlsruhe, Germany) DSX-400 spectrometer operating at resonance frequencies of 162.12 MHz for ^{31}P, 100.72 MHz for ^{13}C, and 40.58 MHz for ^{15}N. Four millimeter magic-angle spinning (MAS) probes tuned to triple resonance (^{1}H, ^{13}C, and ^{31}P) or double resonance [^{1}H and X (X = ^{13}C or ^{15}N)] were used. Low temperatures were achieved using a Kinetics Thermal System (Stone Ridge, NY) XR air-jet sample cooler. Typical ^{1}H, ^{13}C, and ^{31}P 90° pulse lengths were 4.0, 5.0, and 4.5 μs, respectively. ^{13}C, ^{15}N, and ^{31}P chemical shifts were referenced to the ^{13}C signal of the α-Gly CO at 176.49 ppm on the TMS scale, the ^{15}N signal of [^{15}N]acetyl-valine (NAV) at 122.0 ppm on the liquid ammonia scale, and the ^{31}P signal of hydroxylapatite at 2.73 ppm on the phosphoric acid scale, respectively.

^{1}H−^{13}C cross-polarization (CP) was achieved using spin-lock fields of 50 kHz. ^{13}C chemical shifts were assigned using one-dimensional (1D) double-quantum (DQ) filtered experiments and two-dimensional (2D) ^{13}C−^{13}C DARR correlation experiments.[39] DQ excitation and reconversion were achieved using the SPC-5 sequence[40] under 4.5−5.5 kHz MAS. The DARR experiments used a mixing time of 40 ms to establish through-space correlation peaks.

^{13}C−^{1}H dipolar couplings were measured using the DIPSHIFT experiment under spinning speeds of 3.5−5.0 kHz.[41,42] ^{1}H homonuclear decoupling was achieved using the MREV-8 sequence with a ^{1}H 105° pulse length of 4.0 μs.[43] Fitting the t_1 curve gave the apparent C−H dipolar coupling, which was divided by the MREV-8 scaling factor of 0.47 to give the true dipolar coupling. The ratio of the true coupling to the rigid-limit value, 22.7 kHz, gave the order parameter S_{CH}. The model tripeptide, ^{13}C- and ^{15}N-labeled *N*-formyl-Met-Leu-Phe-OH (f-MLF), was used to verify the MREV-8 scaling factor.

Semiquantitative distances from the peptide to the center of the lipid membrane and to water were measured using the 2D ^{13}C-detected ^{1}H spin diffusion experiment. This approach has been used extensively to determine the depth of insertion and water accessibility of membrane peptides and proteins.[26,44−49] The experiment selects the ^{1}H magnetization of mobile lipid

chains and water using a ^{1}H T_2 filter of 0.8−1.0 ms. The selected ^{1}H magnetization is then transferred to the rigid peptide and protein during a mixing period (t_m). The transfer rate depends on the intermolecular distances. The result of ^{1}H spin diffusion to the protein is detected via ^{13}C after a ^{1}H−^{13}C CP step. The buildup of the cross-peak intensities as a function of t_m is fit to give semiquantitative distances. We conducted the ^{1}H spin diffusion experiments under 5 kHz MAS at 308 K for the ReLPS/DEPE samples and 288 K for the POPE/POPG samples. Both temperatures were 3 K below the phase transitions of each membrane and thus gave comparable spin diffusion coefficients. For the POPE/POPG samples, a buildup curve was also measured at 298 K, 7 K above the phase transition temperature, to compare with previous PG-1 data measured at 298 K and to validate the interfacial diffusion coefficient used for distance fitting at 288 K.

^{13}C−^{31}P distances between the peptide and the lipid phosphates were measured using the rotational-echo double-resonance (REDOR) experiment.[50,51] For Cα−^{31}P distances, a 1 ms ^{13}C 180° Gaussian pulse on resonance with the Cα peak was applied in the middle of the REDOR mixing period to refocus the ^{13}C chemical shift and eliminate the ^{13}C−^{13}C scalar couplings.[51] Cζ of Arg does not have a directly bonded ^{13}C; thus, a nonselective 180° pulse was used. A pair of experiments without (S_0) and with (S) ^{31}P pulses was measured for each mixing time. A ^{1}H decoupling field strength of 71 kHz was used during the REDOR period, and the experiments were conducted at 233−237 K under 4.0 or 4.5 kHz MAS. The decay of S/S_0 as a function of mixing time was fit using SIMPSON[52] to obtain the distances. Two-spin (^{13}C−^{31}P) simulations were used for all distance fitting. We have shown before[27] that, for ^{13}C−^{31}P distances shorter than 5 Å, two-spin simulations accurately represent the ^{13}C distance to the nearest ^{31}P, because the average ^{31}P−^{31}P separation in membrane bilayers is much larger (∼10 Å). For apparent two-spin distances of >7 Å, the two-spin distance closely represents, and only slightly overestimates, the vertical distance from the ^{13}C spin to the ^{31}P plane.

RESULTS

In our study, the POPE/POPG membrane was used to mimic the Gram-positive bacterial membrane as well as the inner membrane of Gram-negative bacteria, whereas the ReLPS/DEPE membrane was used to mimic the outer membrane of Gram-negative bacteria. ReLPS and DEPE mix homogeneously because of their similar phase transition temperatures (36 °C for ReLPS[34] and 38 °C for DEPE[53]) and the strong hydrogen bonding capability of the PE headgroup.[54,55]

Membrane Disorder Caused by PG-1 and IB484. We first measured the static ^{31}P spectra of the two types of lipid membranes to assess the membrane disorder caused by IB484. ^{31}P chemical shift anisotropy (CSA) is highly sensitive to the membrane morphology.[32,56−62] Unoriented liquid-crystalline lamellar bilayers exhibit a powder pattern with a uniaxial line shape, whose maximal intensity (90° edge) appears between −12 and −17 ppm. Correspondingly, the span of the powder pattern is 38−50 ppm. In comparison, small isotropic vesicles, micelles, and cubic-phase lipids give rise to an isotropic ^{31}P peak at ∼0 ppm because of lateral diffusion of the lipids over the curved surface of these morphologies or fast tumbling of the vesicles when they are highly hydrated. Finally, hexagonal-phase lipids exhibit a uniaxial line shape that is mirror-symmetric with that of the lamellar bilayer around the isotropic shift, with a maximal intensity of ∼8 ppm.

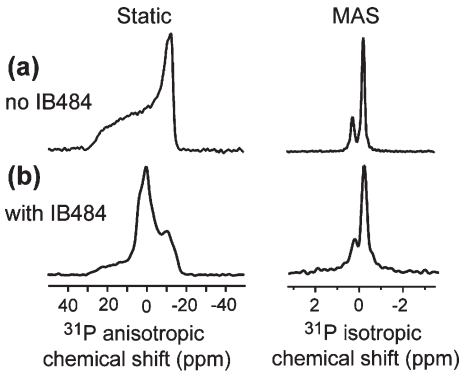

Figure 3. ^{31}P static (left) and MAS (right) spectra of POPE/POPG membranes at 303 K (a) without peptide and (b) with 8 mol % IB484.

Figure 3 shows the static and MAS ^{31}P spectra of the POPE/POPG membrane without and with IB484. While the peptide-free spectrum is characteristic of liquid-crystalline lamellar bilayers, the static spectrum of IB484-containing POPE/POPG membranes exhibits a high 0 ppm isotropic peak superimposed with residual powder intensities, indicating that the bilayer is significantly disrupted by the peptide to form high-curvature isotropic phases. The MAS spectra show that IB484 binding broadens the ^{31}P line widths so that the two lipid signals are no longer well resolved. Thus, IB484 strongly disrupts the POPE/POPG membrane, similar to PG-1,[29,32] consistent with the similar antimicrobial activities of the two peptides toward Gram-positive bacteria (Table 1).

Figure 4 shows static ^{31}P spectra of ReLPS/DEPE membranes in the absence and presence of the peptides and their best-fit simulations to identify the membrane morphologies under the various conditions. The spectra were recorded at 303 and 313 K, which are slightly below and above the phase transition temperature of the membrane, respectively. The spectra of pure DEPE membranes (Figure 4a) show lamellar powder patterns at both temperatures. In contrast, the ReLPS/DEPE (1:5) membrane exhibits a clear isotropic peak (∼15%) in addition to a bilayer powder pattern (Figure 4b) at 303 K, indicating that a small fraction of lipids assembled into small vesicles, micelles, or cubic phases. When the temperature increased to 313 K, the bilayer pattern was replaced by a hexagonal-phase powder pattern, which accounted for ∼88% of the total intensity. This hexagonal phase formation suggests that the LPS acyl chains experience larger disorder relative to the headgroup in the liquid-crystalline phase, thus causing negative curvature strain to the membrane. The result is consistent with previous X-ray diffraction and NMR studies of LPS-related membranes. For example, X-ray diffraction of lipid A membranes detected inverse hexagonal phase in the liquid-crystalline state under a wide range of hydration levels and Mg^{2+} concentrations.[63,64] X-ray diffraction of LPS molecules with varying acyl chain numbers and headgroup sizes[65] showed that whether LPS molecules have cylindrical or conical conformations strongly influences the packing and phase behavior of mixed LPS/phospholipid membranes.

A previous ^{31}P NMR analysis of ReLPS mixtures with phospholipids found that ReLPS forms lamellar bilayers with PE lipids more readily than with phosphocholine (PC) lipids because of the shape complementarity of LPS and PE,[55] and that at 10 mol % ReLPS, only a small isotropic ^{31}P peak was present at

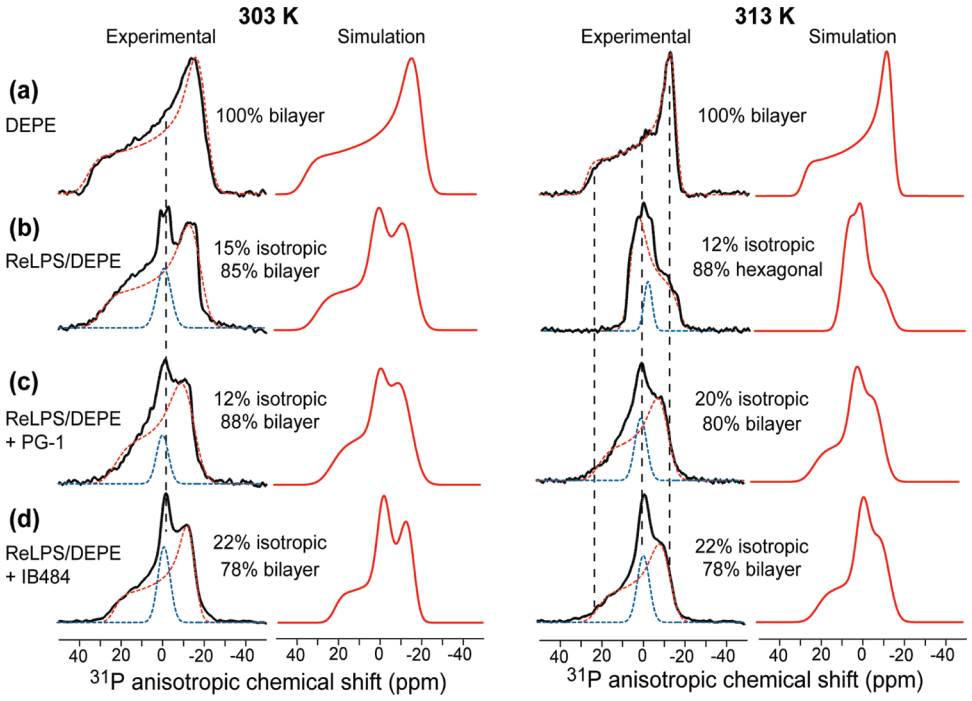

Figure 4. Experimental (black) and simulated (red and blue) static ^{31}P spectra of ReLPS-containing membranes without and with peptides. The spectra were recorded at 303 and 313 K. (a) DEPE spectra. (b) Spectra of ReLPS/DEPE membranes. (c) Spectra of ReLPS/DEPE membranes containing 8 mol % PG-1. (d) Spectra of ReLPS/DEPE membranes containing 8 mol % IB484. Best-fit simulations yield the percentages of each component.

40 °C. However, small- and wide-angle X-ray scattering indicated that the amount of the isotropic phase increases with the LPS concentration and becomes dominant in equimolar mixtures of ReLPS with DPPE/DPPG lipids.[66] The ReLPS/DEPE membrane used here contains 20 mol % ReLPS; thus, the significant but not dominant ^{31}P isotropic peak in the 313 K spectrum is qualitatively consistent with the previous results obtained at 10 and 50% LPS.

Adding PG-1 and IB484 to the LPS membrane removed the hexagonal phase and stabilized the bilayer phase to ~80% of the total intensity (Figure 4c,d).[67] Thus, PG-1 and IB484 counter the negative curvature strain of the LPS-rich membrane. At 303 K, the bilayer powder patterns are ~9 ppm narrower than those of the peptide-free LPS membranes, suggesting that the lipid headgroup conformation may be moderately affected by the peptides to give a different motionally averaged CSAs.[57,68] The ^{31}P powder patterns in the presence of the peptides also show less defined edges, even though the same ^{1}H decoupling field (50 kHz) was applied. We attribute this effect to peptide-induced changes in the lipid diffusion rates, which cause intermediate-time scale broadening of the spectra. Finally, for both PG-1 and IB484, the isotropic peak of the ReLPS/DEPE membrane is smaller than that of the POPE/POPG membrane (Figure 3b),[31] and the difference between the spectra of PG-1- and IB484-containing ReLPS/DEPE membranes is modest compared to the 30-fold MIC difference against Gram-negative bacteria. Thus, we turned to other observables to understand the origin of the different interactions of these two peptides with the LPS membrane.

Conformation and Dynamics of PG-1 and IB484 in Membranes That Mimic Those of Bacteria. We determined the conformation of PG-1 and IB484 in the two lipid membranes by measuring ^{13}C chemical shifts of site-specifically labeled residues. The 2D ^{13}C correlation spectrum of IB484 in POPE/POPG membranes resolved all intraresidue cross-peaks of Arg3 and Val13 (Figure 5a). For the ReLPS/DEPE samples, the 1D ^{13}C spectrum in the absence of the peptides (Figure 5b) showed weak carbohydrate signals in the 60−100 ppm range as expected. The addition of PG-1 and IB484 gave rise to clear peptide ^{13}C signals that were confirmed by DQ filtered spectra (red), which suppressed all natural abundance ^{13}C signals of the lipids. These 1D and 2D spectra readily yielded Cα, Cβ, CO, and Nα chemical shifts of the labeled residues and confirmed the β-sheet conformation of the two peptides in the ReLPS/DEPE membrane. Moreover, no chemical shift or line width changes were observed from 243 to 308 K, and the 308 K ^{13}C spectra showed ~85% of the intensities of the 243 K spectra (data now shown). Thus, PG-1 and IB484 are mostly immobilized in the LPS membranes at physiological temperature.

To quantify the dynamics of IB484 in the two lipid membranes, we measured C−H dipolar couplings. Figure 6 shows the DIPSHIFT data of IB484 in POPE/POPG membranes at 298 K, which is above the phase transition temperature (291 K), and in ReLPS/DEPE membranes at 308 K, slightly below the phase transition temperature (311 K). In both membranes, the Cα sites of Arg3 and Val13 exhibit fast dephasing in the first half of the rotor period, indicating strong C−H dipolar couplings. The best-fit couplings gave a C−H order parameters of ~0.9, indicating that IB484 does not undergo fast motions at these temperatures in the two membranes. The POPE/POPG membrane result was also reproduced at 288 K (Table S1), confirming the lack of fast peptide motion at 298 K. However, the time signals of IB484 showed varying extents of asymmetry between the first and second halves of the rotor period: the intensities at the end of the rotor period were ~72% of the first time point for the POPE/POPG sample at 298 K and ~54% for the ReLPS/DEPE sample at 308 K. This asymmetry is known to be caused by intermediate-time scale motion that interferes with ^{13}C−^{1}H and ^{1}H−^{1}H

dx.doi.org/10.1021/bi101975v |*Biochemistry* 2011, 50, 2072–2083

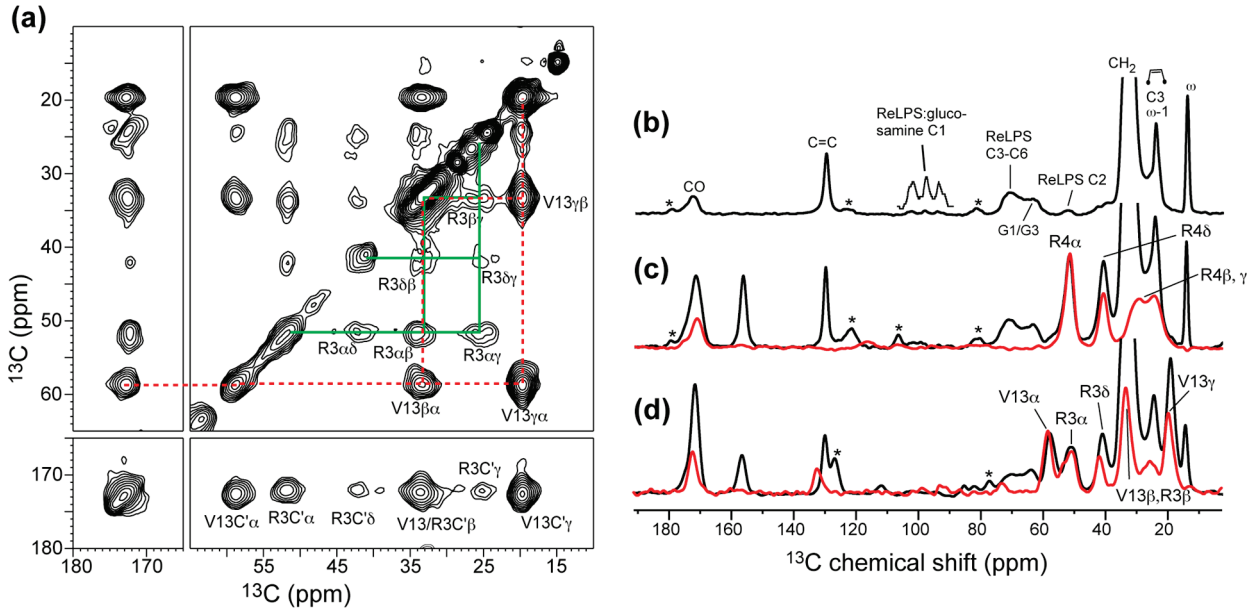

Figure 5. ^{13}C chemical shifts of PG-1 and IB484 in ReLPS/DEPE membranes. (a) Representative 2D ^{13}C−^{13}C DARR spectrum (40 ms mixing) of Arg3- and Val13-labeled IB484 in POPE/POPG membranes at 263 K. The 2D spectrum was recorded for 19 h with a maximal t_1 evolution time of 6 ms, 218 t_1 slices, and 160 scans per slice. (b) 1D ^{13}C CP-MAS spectra of ReLPS/DEPE membranes. Asterisks indicate spinning sidebands. (c) ^{13}C CP-MAS spectrum (black) and ^{13}C DQ filtered spectrum (red) of PG-1 in ReLPS/DEPE membranes. (d) ^{13}C CP-MAS spectrum (black) and ^{13}C DQ filtered spectrum (red) of IB484 in ReLPS/DEPE membranes. The 1D spectra were recorded between 237 and 253 K under 4−5 kHz MAS. The 1D DQ filtered spectra were recorded with 2560 scans.

dipolar couplings and MAS.[69] The larger intensity reduction in the ReLPS/DEPE membrane suggests that IB484 may bind more superficially to this membrane or may be less oligomerized compared to its behavior in the POPE/POPG membrane. Comparison with reported DIPSHIFT curves for various motional rates and amplitudes[69] suggests that the intermediate-time scale motion of IB484 may occur in the 2−10 kHz regime, although the exact rates and amplitudes depend on the motional geometry and are outside the scope of this study.

Interestingly, the POPE/POPG membrane-bound PG-1 also exhibited noticeable intensity asymmetry in the DIPSHIFT data (Figure 6c), indicating that intermediate-time scale motion was already present in the wild-type peptide. Table S1 of the Supporting Information summarizes the C−H order parameters and the apparent T_2 decay constants (T_2*) of the four peptide/lipid combinations. In the ReLPS/DEPE membrane, PG-1 has a much longer T_2* (1.45 ms) or much less DIPSHIFT asymmetry (Figure 6d) than IB484 (0.34 ms), suggesting that the wild-type peptide binds more tightly to the LPS membrane than the mutant.

Depth of Insertion from ^{13}C-Detected ^{1}H Spin Diffusion. To determine the depth of insertion of the two peptides, we conducted 2D ^{13}C-detected ^{1}H spin diffusion experiments. The spin diffusion spectra were recorded for POPE/POPG samples at 288 K and ReLPS/DEPE samples at 308 K, ∼3 K below the corresponding phase transition temperatures. The similar reduced temperatures make ^{1}H spin diffusion coefficients similar so that buildup curves can be compared between the two types of membranes. On the basis of previous calibrations, we used the following diffusion coefficients to extract lipid−protein and water−protein distances: D_L = 0.012 nm^2/ms for the lipid phase, D_W = 0.03 nm^2/ms for water, and D_P = 0.3 nm^2/ms for the peptides.[26,45,48] For the lipid−protein interface, we used a D_{int} of 0.005 nm^2/ms, as verified below.

Figure 7a shows a representative 2D ^{13}C−^{1}H correlation spectrum of IB484 in ReLPS/DEPE membranes. With a 100 ms mixing time, peptide−CH_2 and peptide−water cross-peaks were clearly observed at ^{1}H chemical shifts of 1.3 and 4.8 ppm, respectively. The sum of the ^{1}H cross-peaks of Cα of Arg3 and Cα of Val13 as a function of mixing time is shown in Figure 7b. The cross-peak intensity buildup as a function of mixing time is shown in Figure 8a for IB484 in the two membranes. The lipid CH_2 buildup curve rises much more slowly in the ReLPS/DEPE membrane than in the POPE/POPG membrane. The latter curve is best fit to a 2 Å distance, indicating that IB484 is inserted into the center of the POPE/POPG membrane. The lipid chain CH_3 buildup curve (not shown) is similar to the CH_2 curve,[44] confirming that the mutant is fully inserted across the membrane. Water spin diffusion to IB484 is also fast in the POPE/POPG membrane. Because the length of IB484 (∼26 Å) is shorter than the POPE/POPG P−P thickness (∼45 Å), fast spin diffusion from both water and lipid acyl chains suggests permeation of water into the membrane. In comparison, the CH_2 buildup curve for the ReLPS/DEPE membrane is best fit to a distance of 7 Å, indicating that IB484 is only partly inserted into the LPS membrane. At the same time, the water buildup curve is also slower in the ReLPS/DEPE membrane than in the POPE/POPG membrane, corresponding to an ∼5 Å distance.

The ^{1}H spin diffusion curves of PG-1 and IB484 in the ReLPS/DEPE membrane are compared in Figure 8b. Spin diffusion from both lipid CH_2 and water to PG-1 is rapid (2 Å), indicating TM insertion of the peptide. The lipid CH_2 buildup curve is clearly faster for PG-1 than for IB484, supporting deeper insertion of the more cationic PG-1. Water spin diffusion to PG-1 is modestly faster than to IB484 in the LPS membrane. Because the PG-1 buildup curves were extracted from the Cα signal of Arg4, which contains labile side chain protons that can readily exchange with water, we analyzed the water spin diffusion curve to IB484 using

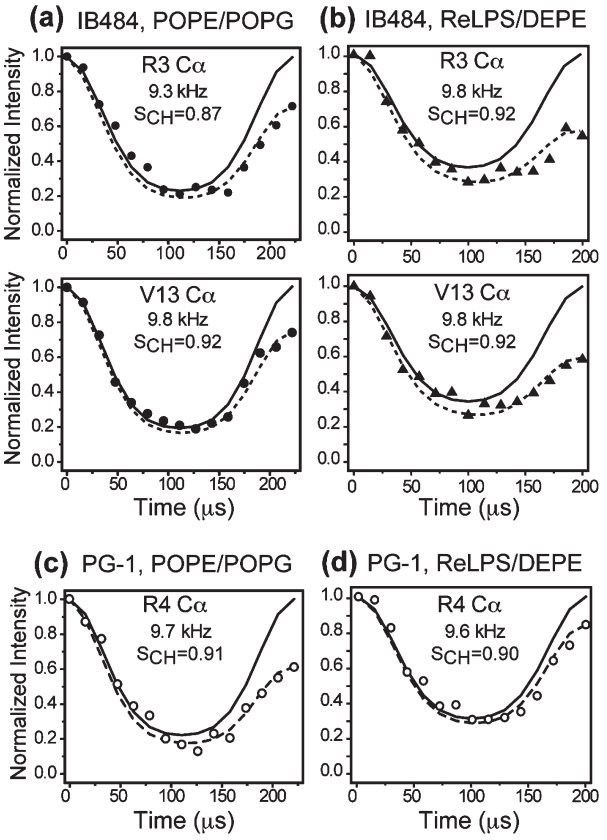

Figure 6. C−H order parameters of IB484 and PG-1 in different membranes by 2D DIPSHIFT experiments. (a) IB484 in POPE/POPG membranes at 298 K under 4.5 kHz MAS. (b) IB484 in ReLPS/DEPE membranes at 308 K under 5 kHz MAS. (c) PG-1 in POPE/POPG membranes at 298 K under 4.5 kHz MAS. (d) PG-1 in ReLPS/DEPE membrane at 308 K under 5.0 kHz MAS. Solid and dashed lines are best-fit simulations without and with T_2 decays, respectively.

only the Arg3 Cα intensity. The resulting buildup curve (empty circles) is the same as that obtained using the combined Arg3 and Val13 intensities (Figure 8b, filled circles), confirming that IB484 is farther from water than PG-1.

The spin diffusion buildup curves described above were fit using an interfacial diffusion coefficient of 0.005 nm^2/ms, which is larger than the value of 0.002 nm^2/ms used previously for liquid-crystalline membranes.[45] This interfacial diffusion coefficient is a sensitive parameter in the distance fitting and is only semiquantitatively estimated on the basis of $^1H-^1H$ dipolar couplings.[48] Although the higher D_{int} was consistent with the moderate gel-phase nature (3 K below the phase transition temperature) of the membranes in our experiments, we further verified the interfacial diffusion coefficient by repeating the spin diffusion experiment for POPE/POPG membrane-bound IB484 at 298 K. Figure S1a of the Supporting Information compares the CH_2 buildup curves of IB484 and PG-1 at 298 K in the POPE/POPG membrane.[26] The two curves superimpose well, indicating that the two peptides have similar distances to the center of the POPE/POPG membrane. Using a D_{int} of 0.00175 nm^2/ms, which was previously estimated for PG-1, we obtained the 2 Å distance for IB484, which is identical to the result at 288 K. Figure S1b of the Supporting Information compares the buildup curves of IB484 at 288 and 298 K in the POPE/POPG membrane. As expected, higher temperature slowed ^1H spin diffusion because

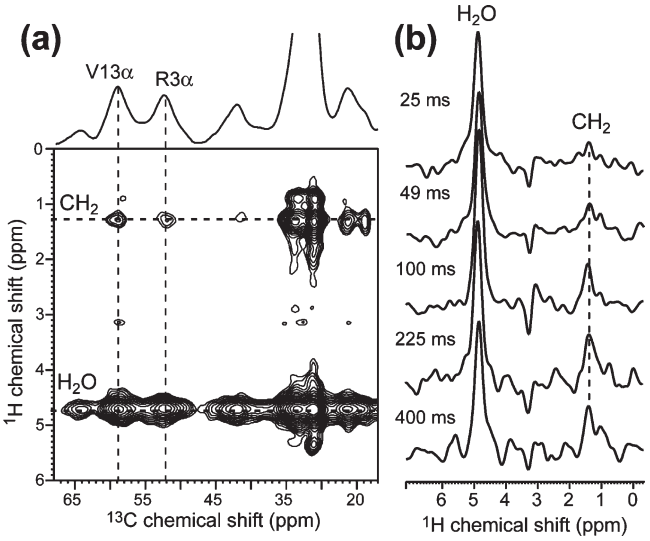

Figure 7. 2D ^{13}C-detected ^1H spin diffusion spectra of IB484 in the ReLPS/DEPE membrane to determine the peptide's depth of insertion. (a) Representative 2D spectrum, measured with a 100 ms mixing time. (b) Sum of the Arg3 and Val13 Cα−^1H cross-peaks as a function of mixing time.

of the lower membrane viscosity, but the intrinsic depth of the peptide is the same within this narrow temperature range. Thus, the choice of 0.005 nm^2/ms for D_{int} at 288 K is consistent with the higher D_{int} value for liquid-crystalline POPE/POPG membranes, and IB484 is inserted into the hydrophobic center of this membrane.

Guanidinium Phosphate $^{13}C-^{31}P$ Distances. To understand how Arg residues in the two peptides interact with the lipids, we measured $^{13}C-^{31}P$ distances in both the LPS and regular phospholipid membranes. Figure 9a shows the REDOR data of PG-1 in ReLPS/DEPE membranes and compares them with the previously reported POPE/POPG results.[27] In the POPE/POPG membrane, Arg4 has a short Cζ−P distance of 5.7 Å indicative of guanidinium phosphate complexation and a Cα−P distance of 6.5 Å.[27] These distances suggest toroidal pore formation by PG-1 in POPE/POPG membranes.[26,27] In the ReLPS/DEPE membrane, the Arg4 Cζ−P distance increased to 6.9 Å while the Cα−P distance increased to 8.0 Å. Thus, the guanidinium phosphate salt bridge no longer exists in the LPS-bound PG-1. Because the ^1H spin diffusion data indicate TM insertion of PG-1 into this membrane, the lack of short $^{13}C-^{31}P$ distances suggests that there are fewer or no lipid headgroups in the center of the membrane, which is consistent with the limited isotropic intensity in the static ^{31}P spectrum of the PG-1-containing LPS membrane (Figure 4c).

Figure 9b shows the REDOR curves of IB484 in POPE/POPG (empty symbols) and ReLPS/DEPE membranes (filled symbols), and a representative pair of REDOR spectra is shown in Figure 9c. The Arg3 Cζ−P dephasing in both membranes is fit well by a Gaussian distribution of distances centered at 5.7 Å with a half-width of 1.5 Å. Thus, on average Arg3 has close contact with the lipid phosphates in both membranes. For the backbone atoms, Arg3 shows a Cα−P distance of 6.4 Å in the LPS membrane and 7.4 Å in the POPE/POPG membrane, while Val13 has a Cα−P distance of 7.6−7.7 Å in both membranes. The accuracy of the REDOR experiment is verified by the rapid dephasing of the lipid glycerol G1 and G3 peak (63.5 ppm),

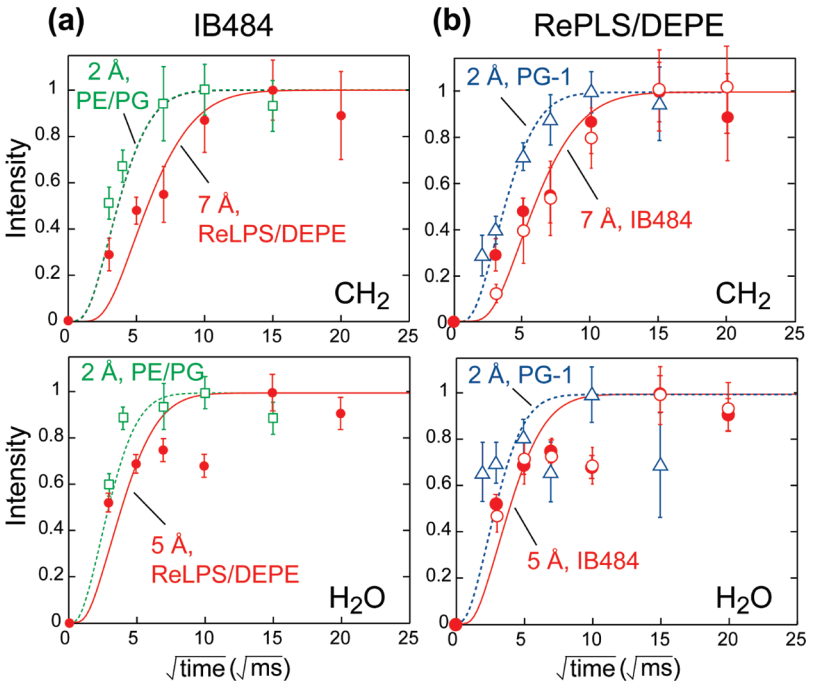

Figure 8. Analysis of ^{1}H spin diffusion data of PG-1 and IB484 in two lipid membranes. (a) Buildup curves of IB484 in ReLPS/DEPE (filled circles) and POPE/POPG (empty squares) membranes, measured at 308 and 288 K, respectively. The intensity is the sum of the Arg3 and Val13 Cα−^{1}H cross-peaks. The top panel shows spin diffusion from lipid CH_2 protons to the peptide and the bottom panel spin diffusion from water to the peptide. (b) Buildup curves of IB484 (circles) and PG-1 (triangles) in ReLPS/DEPE membranes at 308 K. For the IB484 data, the sum of the Arg3 and Val13 Cα intensity is shown as filled circles while the Arg3 Cα intensity is shown as empty circles.

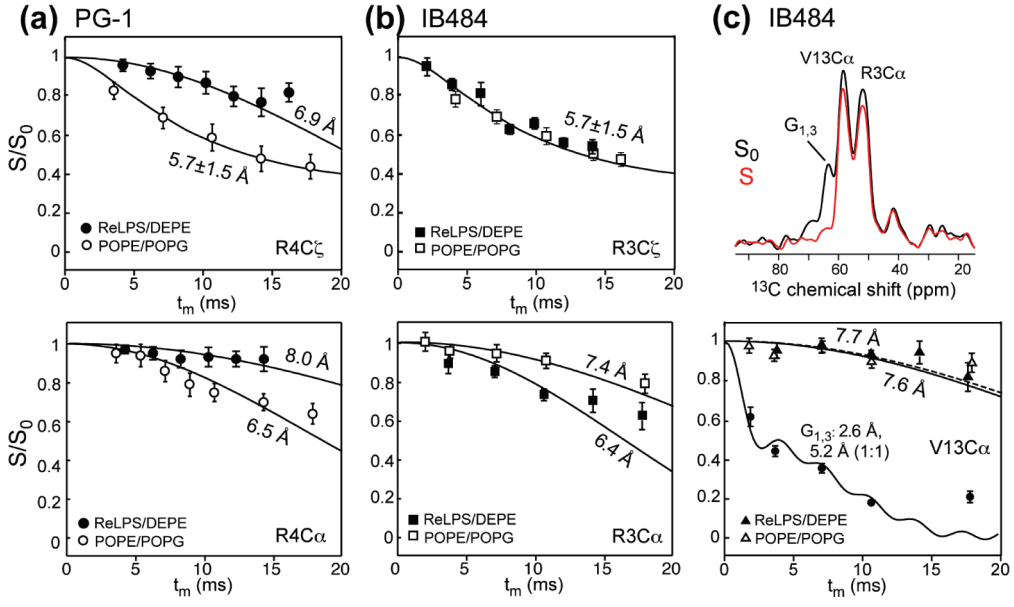

Figure 9. ^{13}C−^{31}P REDOR data of PG-1 and IB484. (a) Distances from PG-1 Arg4 Cα and Cζ to ^{31}P in the ReLPS/DEPE membrane (filled symbols). The POPE/POPG data (empty symbols) are superimposed.[27] (b) IB484 Arg3 Cα and Cζ and Val13 Cα data in the ReLPS/DEPE membrane (filled symbols) vs the POPE/POPG membrane (empty symbols). (c) Representative REDOR S_0 and S spectra of IB484 in the POPE/POPG membrane. The mixing time was 10.7 ms. The REDOR experiments were conducted at 233−237 K under 4.0 or 4.5 kHz MAS.

which fit to a 1:1 combination of a 2.6 and 5.2 Å distance, consistent with the short intramolecular distances from these carbons to ^{31}P. All measured ^{13}C−^{31}P distances are summarized in Table 2.

Although short guanidinium phosphate distances were found for IB484 in both lipid membranes, the different depths of the peptide obtained from the ^{1}H spin diffusion experiment indicate different reasons for the short ^{13}C−^{31}P distances. The mutant is shallowly inserted into the ReLPS/DEPE membrane and is thus in the proximity of the phosphate groups on the membrane surface. In contrast, the peptide is fully inserted across the POPE/POPG membrane; thus, the relatively short Cζ−P distance of Arg3 must result from phosphate groups embedded in

dx.doi.org/10.1021/bi101975v |*Biochemistry* 2011, 50, 2072–2083

the hydrophobic region of the membrane, as in toroidal pores. The 1.3 Å difference in the distances from the Cα atoms of Arg3 and Val13 to ^{31}P in the LPS membrane suggests that the C-terminus may be more deeply inserted into the membrane than the N-terminus, due to the more hydrophobic nature of the C-terminal strand compared to the N-terminal strand (Figure 2a).

DISCUSSION

Understanding the Gram selectivity of AMPs is important for designing new antibiotics that selectively target resistant bacteria. Previous studies of AMPs in LPS micelles or intact Gram-negative bacteria suggested the lack of peptide insertion to be the cause for the weaker antimicrobial activities of Gram-negative-inactive AMPs.[17−19] However, molecular structures of AMPs in LPS-containing lipid bilayers have not been reported. This study addresses the mechanism of Gram selectivity by comparing the structures of PG-1 and a mutant in Gram-positive and Gram-negative mimetic lipid membranes. On the basis of our data, we propose four structural models (Figure 10 and Table S2 of the Supporting Information) that explain the different antimicrobial activities of the two peptides.

Both PG-1 and IB484 adopt a robust β-hairpin fold because of the disulfide bond constraints. Previous solid-state NMR data and MD simulations showed that the wild-type β-hairpins assemble into oligomeric TM β-barrels in POPE/POPG membranes,[26,70,71] which lead to toroidal pore defects (Figure 10a).[27] The current data show that the charge-reduced mutant is similarly inserted into the POPE/POPG membrane and also exhibits short Arg Cζ−P distances that are diagnostic of toroidal pores (Figure 10c). The membrane disorder is consistent with the ^{31}P NMR line shape of mutant-bound POPE/POPG membranes, which exhibited a high isotropic peak (Figure 3b). It is also consistent with the similar antimicrobial activities of IB484 and PG-1 against Gram-positive bacteria (Table 1).

Guanidinium phosphate salt bridges have now been observed for many cationic membrane peptides, including the antimicrobial peptides PG-1[27] and human α-defensin 1,[72] the cell-penetrating peptides penetratin[73,74] and HIV TAT,[75] and the S4 helix of the KvAP potassium channel.[76] Solid-state NMR provided the most direct means of identifying the existence of guanidinium phosphate complexation through distance measurements between the Arg Cζ and lipid ^{31}P. In addition to interaction with the lipid phosphates, the guanidinium ion can also form hydrogen bonds with water.[77,78] Both interactions shield the positive charge from the hydrophobic lipid chains, thus facilitating membrane insertion of these peptides. IB484 exhibits clear guanidinium phosphate interactions in POPE/POPG membranes, suggesting that even with only two Arg residues, the peptide is able to cause some phospholipids to reorient to lower the free energy barrier of insertion of the peptide into the hydrophobic region of the membrane.

While both PG-1 and IB484 induce toroidal pores in the POPE/POPG membrane, they show different Arg Cα−-P distances: the IB484 Arg3 Cα atom exhibited a 1 Å longer distance (7.4 Å) than the corresponding Arg4 Cα atom in PG-1 (6.5 Å). This difference suggests that fewer phosphate groups may reorient to contact the Arg in the mutant, as a result of the weaker electrostatic interaction of the membrane with the +3 charged mutant compared to the +6 charged PG-1. The distance difference is consistent with the 2-fold weaker antimicrobial

Table 2. ^{13}C−^{31}P Distances of PG-1 and IB484 in POPE/POPG and ReLPS/DEPE Membranes

peptide	residue	site	POPE/POPG	ReLPS/DEPE
PG-1	Arg4	Cζ	5.7 ± 1.5 [27]	6.9
		Cα	6.5 [27]	8.0
IB484	Arg3	Cζ	5.7 ± 1.5	5.7 ± 1.5
		Cα	7.4	6.4
	Val13	Cα	7.6	7.7

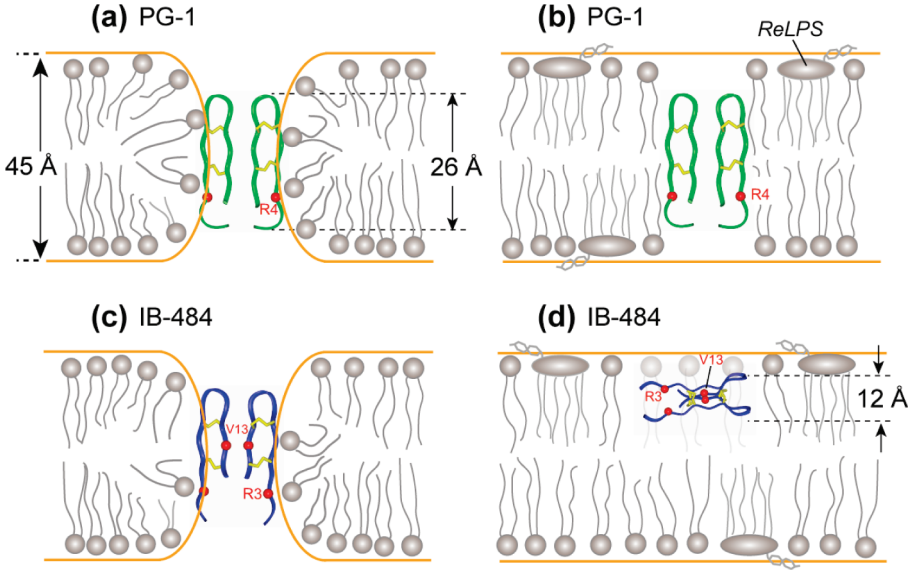

Figure 10. Structural models of PG-1 and IB484 in ReLPS/DEPE and POPE/POPG membranes. (a) In the POPE/POPG membrane, PG-1 is TM and leads to toroidal pores with strong orientational disorder.[26,27] (b) In the ReLPS/DEPE membrane, PG-1 is TM and causes barrel-stave pores with little lipid orientational disorder. (c) In the POPE/POPG membrane, IB484 is TM and causes toroidal pores with moderate lipid disorder. (d) In the ReLPS/DEPE membrane, IB484 is partially inserted without causing lipid disorder. The peptide cannot subsequently cross into the cytoplasmic membrane, thus explaining its weak antimicrobial activity against Gram-negative bacteria.

activity of IB484 than PG-1 toward Gram-positive MRSA (Table 1).

In ReLPS/DEPE membranes, ^{1}H spin diffusion data indicate that PG-1 lies close to both water and lipid chains and is thus inserted in a TM fashion.[26] However, the peptide exhibits much longer distances from Arg4 to ^{31}P compared to the distances in the POPE/POPG membrane. Although only Arg4 is measured in this study, distances from other Arg residues to ^{31}P will not provide additional information about the peptide−lipid interaction, because the other five Arg residues in PG-1 are located at the hairpin tip and at the N- and C-termini; thus, they are close to the lipid ^{31}P regardless of whether the peptide adopts a TM or a surface-bound structure. Among the six Arg residues, Arg4 is closest to the hydrophobic middle of the β-hairpin and is thus most sensitive to the absence or presence of toroidal pore defects. The combination of ^{1}H spin diffusion and ^{13}C−^{31}P distance data indicates that PG-1 causes TM pores of the barrel-stave type in the ReLPS/DEPE membrane (Figure 10b), where the lipid molecules maintain their regular orientation parallel to the membrane normal. The relative lack of orientational disorder is confirmed by the ^{31}P spectra (Figure 4c). These TM pores, presumably filled with water, shield the Arg residues from the hydrophobic lipid chains and at the same time provide a conduit for translocation of more PG-1 molecules into the cytoplasmic membrane, where actual cell killing occurs. The phase behavior of the ReLPS/DEPE membrane is complex in the absence of the peptide and has not been fully explored as a function of temperature and composition.[55,66] Nevertheless, the ^{31}P spectra in Figure 4 clearly show that the ReLPS/DEPE membrane has a significant level of curvature strain in the liquid-crystalline phase that is reduced in the gel phase. Thus, chain disorder plays a significant role in the lipid packing of the ReLPS/DEPE membrane. Binding of either peptide to the LPS membrane restored the lamellar bilayer at high temperature, which may proceed by chain rigidification or by the peptides counteracting the negative curvature strain of the lipids.

The biggest difference between the mutant and wild-type PG-1 lies in their depths of insertion into the ReLPS/DEPE membrane. The mutant cannot insert into the center of the LPS membrane, as shown by the slower ^{1}H spin diffusion from the lipid CH_2; thus, it cannot cross further into the cytoplasmic membrane. The shallow insertion of IB484 into the LPS membrane, in contrast to its TM orientation in the POPE/POPG membrane, may result from a combination of the large oligosaccharide moiety, the presence of six acyl chains, and the divalent cations that neutralize the LPS negative charges. These structural features serve to make the LPS-rich membrane more rigid and less permeable than regular phospholipid membranes (Figure 2). The fact that wild-type PG-1 still inserts into the ReLPS/DEPE membrane, despite the high membrane viscosity and impermeability, must then be attributed to the higher charge of the wild-type peptide and the stronger electrostatic interaction, but the more rigid LPS molecules cannot reorient to neutralize the Arg residues of the inserted PG-1; thus, no toroidal pores are observed. For IB484, the smaller number of cationic residues (two Arg residues and one Lys) weakens the electrostatic attraction with the membrane, hence abolishing TM insertion. In the asymmetric outer membrane of real Gram-negative bacterial cells, the LPS molecules are almost exclusively located in the outer leaflet. Therefore, resistance against peptide insertion may be stronger and a higher cationicity may be required for potent antimicrobial activities.

In conclusion, the solid-state NMR data obtained here indicate that Gram selectivity among β-hairpin AMPs is largely the result of different insertion depths, which depend on the degree of peptide binding to the membrane, which is in turn determined by the Arg density of the peptides. Having a sufficient number of Arg residues facilitates binding of the peptide to and translocation of the peptide across the LPS membrane of Gram-negative bacteria, allowing subsequent disruption of the inner cytoplasmic membrane.

■ ASSOCIATED CONTENT

Supporting Information. Tables of dipolar order parameters and NMR constraints and additional ^{1}H spin diffusion data. This material is available free of charge via the Internet at http://pubs.acs.org.

■ AUTHOR INFORMATION

Corresponding Author

*Department of Chemistry, Iowa State University, Ames, IA 50011. Telephone: (515) 294-3521. Fax: (515) 294-0105. E-mail: mhong@iastate.edu.

Funding Sources

This work was supported by Grant GM066976 from the National Institutes of Health (to M.H.).

■ ABBREVIATIONS

AMP, antimicrobial peptide; POPE, 1-palmitoyl-2-oleoyl-*sn*-glycero-3-phosphoethanolamine; POPG, 1-palmitoyl-2-oleoyl-*sn*-glycero-3-phosphatidylglycerol; LPS, lipopolysaccharide; DEPE, 1,2-dielaidoyl-*sn*-glycero-3-phosphoethanolamine; MAS, magic-angle spinning; CP, cross-polarization; DARR, dipolar-assisted rotational resonance; DIPSHIFT, dipolar-chemical-shift correlation; REDOR, rotational-echo double-resonance.

■ REFERENCES

(1) Fischbach, M. A., and Walsh, C. T. (2009) Antibiotics for emerging pathogens. *Science 325*, 1089–1093.

(2) Levy, S. B., and Marshall, B. (2004) Antibacterial resistance worldwide: Causes, challenges and responses. *Nat. Med. 10*, S122–S129.

(3) Hancock, R. E., and Sahl, H. G. (2006) Antimicrobial and host-defense peptides as new anti-infective therapeutic strategies. *Nat. Biotechnol. 24*, 1551–1557.

(4) Zasloff, M. (2002) Antimicrobial peptides of multicellular organisms. *Nature 415*, 389–395.

(5) Brogden, K. A. (2005) Antimicrobial peptides: Pore formers or metabolic inhibitors in bacteria?. *Nat. Rev. Microbiol. 3*, 238–250.

(6) Tang, M., and Hong, M. (2009) Structure and mechanism of β-hairpin antimicrobial peptides in lipid bilayers from solid-state NMR spectroscopy. *Mol. Biosyst. 5*, 317–322.

(7) Epand, R. M., and Vogel, H. J. (1999) Diversity of antimicrobial peptides and their mechanisms of action. *Biochim. Biophys. Acta 1462*, 11–28.

(8) Huang, H. W. (2000) Action of antimicrobial peptides: Two-state model. *Biochemistry 39*, 8347–8352.

(9) Kagan, B. L., Selsted, M. E., Ganz, T., and Lehrer, R. I. (1990) Antimicrobial defensin peptides form voltage-dependent ion-permeable channels in planar lipid bilayer membranes. *Proc. Natl. Acad. Sci. U.S.A. 87*, 210–214.

(10) Westerhoff, H. V., Juretić, D., Hendler, R. W., and Zasloff, M. (1989) Magainins and the disruption of membrane-linked free-energy transduction. *Proc. Natl. Acad. Sci. U.S.A. 86*, 6597–6601.

(11) Sperandeo, P., Dehò, G., and Polissi, A. (2009) The lipopolysaccharide transport system of Gram-negative bacteria. *Biochim. Biophys. Acta 1791*, 594–602.

(12) Rosenfeld, Y., and Shai, Y. (2006) Lipopolysaccharide (endotoxin)-host defense antibacterial peptides interactions: Role in bacterial resistance and prevention of sepsis. *Biochim. Biophys. Acta 1758*, 1513–1522.

(13) Lehrer, R. I., Barton, A., Daher, K. A., Harwig, S. S., Ganz, T., and Selsted, M. E. (1989) Interaction of human defensins with *Escherichia coli*. Mechanism of bactericidal activity. *J. Clin. Invest. 84*, 553–561.

(14) Mares, J., Kumaran, S., Gobbo, M., and Zerbe, O. (2009) Interactions of lipopolysaccharide and polymyxin studied by NMR spectroscopy. *J. Biol. Chem. 284*, 11498–11506.

(15) Hancock, R. E., and Scott, M. G. (2000) The role of antimicrobial peptides in animal defenses. *Proc. Natl. Acad. Sci. U.S.A. 97*, 8856–8861.

(16) Raetz, C. R., Garrett, T. A., Reynolds, C. M., Shaw, W. A., Moore, J. D., Smith, D. C., Ribeiro, A. A., Murphy, R. C., Ulevitch, R. J., Fearns, C., Reichart, D., Glass, C. K., Benner, C., Subramaniam, S., Harkewicz, R., Bowers-Gentry, R. C., Buczynski, M. W., Cooper, J. A., Deems, R. A., and Dennis, E. A. (2006) Kdo2-Lipid A of *Escherichia coli*, a defined endotoxin that activates macrophages via TLR-4. *J. Lipid Res. 47*, 1097–1111.

(17) Bhunia, A., Domadia, P. N., Torres, J., Hallock, K. J., Ramamoorthy, A., and Bhattacharjya, S. (2010) NMR structure of pardaxin, a pore-forming antimicrobial peptide, in lipopolysaccharide micelles: Mechanism of outer membrane permeabilization. *J. Biol. Chem. 285*, 3883–3895.

(18) Hammer, M. U., Brauser, A., Olak, C., Brezesinski, G., Goldmann, T., Gutsmann, T., and Andrä, J. (2010) Lipopolysaccharide interaction is decisive for the activity of the antimicrobial peptide NK-2 against *Escherichia coli* and *Proteus mirabilis*. *Biochem. J. 427*, 477–488.

(19) Rosenfeld, Y., Barra, D., Simmaco, M., Shai, Y., and Mangoni, M. L. (2006) A synergism between temporins toward Gram-negative bacteria overcomes resistance imposed by the lipopolysaccharide protective layer. *J. Biol. Chem. 281*, 28565–28574.

(20) Zhang, L., Scott, M. G., Yan, H., Mayer, L. D., and Hancock, R. E. (2000) Interaction of polyphemusin I and structural analogs with bacterial membranes, lipopolysaccharide, and lipid monolayers. *Biochemistry 39*, 14504–14514.

(21) Lienkamp, K., Kumar, K. N., Som, A., Nüsslein, K., and Tew, G. N. (2009) "Doubly selective" antimicrobial polymers: How do they differentiate between bacteria?. *Chem.—Eur. J. 15*, 11710–11714.

(22) Böhling, A., Hagge, S. O., Roes, S., Podschun, R., Sahly, H., Harder, J., Schröder, J. M., Grötzinger, J., Seydel, U., and Gutsmann, T. (2006) Lipid-specific membrane activity of human β-defensin-3. *Biochemistry 45*, 5663–5670.

(23) Bellm, L., Lehrer, R. I., and Ganz, T. (2000) Protegrins: New antibiotics of mammalian origin. *Expert Opin. Invest. Drugs 9*, 1731–1742.

(24) Tam, J. P., Wu, C., and Yang, J. L. (2000) Membranolytic selectivity of cystine-stabilized cyclic protegrins. *Eur. J. Biochem. 267*, 3289–3300.

(25) Chen, J., Falla, T. J., Liu, H., Hurst, M. A., Fujii, C. A., Mosca, D. A., Embree, J. R., Loury, D. J., Radel, P. A., Cheng, C. C., Gu, L., and Fiddes, J. C. (2000) Development of protegrins for the treatment and prevention of oral mucositis: Structure-activity relationships of synthetic protegrin analogues. *Biopolymers 55*, 88–98.

(26) Mani, R., Cady, S. D., Tang, M., Waring, A. J., Lehrer, R. I., and Hong, M. (2006) Membrane-dependent oligomeric structure and pore formation of a β-hairpin antimicrobial peptide in lipid bilayers from solid-state NMR. *Proc. Natl. Acad. Sci. U.S.A. 103*, 16242–16247.

(27) Tang, M., Waring, A. J., and Hong, M. (2007) Phosphate-Mediated Arginine Insertion into Lipid Membranes and Pore Formation by a Cationic Membrane Peptide from Solid-State NMR. *J. Am. Chem. Soc. 129*, 11438–11446.

(28) Mani, R., Tang, M., Wu, X., Buffy, J. J., Waring, A. J., Sherman, M. A., and Hong, M. (2006) Membrane-bound dimer structure of a β-hairpin antimicrobial peptide from rotational-echo double-resonance solid-state NMR. *Biochemistry 45*, 8341–8349.

(29) Yamaguchi, S., Hong, T., Waring, A., Lehrer, R. I., and Hong, M. (2002) Solid-state NMR investigations of peptide-lipid interaction and orientation of a β-sheet antimicrobial peptide, protegrin. *Biochemistry 41*, 9852–9862.

(30) Buffy, J. J., Waring, A. J., Lehrer, R. I., and Hong, M. (2003) Immobilization and aggregation of the antimicrobial peptide protegrin-1 in lipid bilayers investigated by solid-state NMR. *Biochemistry 42*, 13725–13734.

(31) Mani, R., Buffy, J. J., Waring, A. J., Lehrer, R. I., and Hong, M. (2004) Solid-state NMR investigation of the selective disruption of lipid membranes by protegrin-1. *Biochemistry 43*, 13839–13848.

(32) Mani, R., Waring, A. J., Lehrer, R. I., and Hong, M. (2005) Membrane-disruptive abilities of β-hairpin antimicrobial peptides correlate with conformation and activity: A ^{31}P and ^{1}H NMR study. *Biochim. Biophys. Acta 1716*, 11–18.

(33) Wi, S., and Kim, C. (2008) Pore structure, thinning effect, and lateral diffusive dynamics of oriented lipid membranes interacting with antimicrobial peptide protegrin-1: ^{31}P and ^{2}H solid-state NMR study. *J. Phys. Chem. B 112*, 11402–11414.

(34) Sasaki, H., and White, S. H. (2008) Aggregation Behavior of an Ultra-Pure Lipopolysaccharide that Stimulates TLR-4 Receptors. *Biophys. J. 95*, 986–993.

(35) Harwig, S. S., Swiderek, K. M., Lee, T. D., and Lehrer, R. I. (1995) Determination of disulphide bridges in PG-2, an antimicrobial peptide from porcine leukocytes. *J. Pept. Sci. 1*, 207–215.

(36) Aumelas, A., Mangoni, M., Roumestand, C., Chiche, L., Despaux, E., Grassy, G., Calas, B., and Chavanieu, A. (1996) Synthesis and solution structure of the antimicrobial peptide protegrin-1. *Eur. J. Biochem. 237*, 575–583.

(37) Fahrner, R. L., Dieckmann, T., Harwig, S. S., Lehrer, R. I., Eisenberg, D., and Feigon, J. (1996) Solution structure of protegrin-1, a broad-spectrum antimicrobial peptide from porcine leukocytes. *Chem. Biol. 3*, 543–550.

(38) Raetz, C. R., and Whitfield, C. (2002) Lipopolysaccharide Endotoxins. *Annu. Rev. Biochem. 71*, 635–700.

(39) Takegoshi, K., Nakamura, S., and Terao, T. (2001) ^{13}C−^{1}H dipolar-assisted rotational resonance in magic-angle spinning NMR. *Chem. Phys. Lett. 344*, 631–637.

(40) Hohwy, M., Rienstra, C. M., Jaroniec, C. P., and Griffinb, R. G. (1999) Fivefold symmetric homonuclear dipolar recoupling in rotating solids: Application to double quantum spectroscopy. *J. Chem. Phys. 110*, 7983–7992.

(41) Munowitz, M. G., Griffin, R. G., Bodenhausen, G., and Huang, T. H. (1981) Two-dimensional rotational spin-echo nuclear magnetic resonance in solids: Correlation of chemical shift and dipolar interactions. *J. Am. Chem. Soc. 103*, 2529–2533.

(42) Hong, M., Gross, J. D., Rienstra, C. M., Griffin, R. G., Kumashiro, K. K., and Schmidt-Rohr, K. (1997) Coupling Amplification in 2D MAS NMR and Its Application to Torsion Angle Determination in Peptides. *J. Magn. Reson. 129*, 85–92.

(43) Rhim, W. K., Elleman, D. D., and Vaughan, R. W. (1973) Analysis of multiple pulse NMR in solids. *J. Chem. Phys. 59*, 3740–3749.

(44) Tang, M., Waring, A. J., and Hong, M. (2009) Effects of arginine density on the membrane-bound structure of a cationic antimicrobial peptide from solid-state NMR. *Biochim. Biophys. Acta 1788*, 514–521.

(45) Luo, W., and Hong, M. (2010) Conformational changes of an ion channel detected through water-protein interactions using solid-state NMR spectroscopy. *J. Am. Chem. Soc. 132*, 2378–2384.

(46) Ader, C., Schneider, R., Seidel, K., Etzkorn, M., Becker, S., and Baldus, M. (2009) Structural rearrangements of membrane proteins probed by water-edited solid-state NMR spectroscopy. *J. Am. Chem. Soc. 131*, 170–176.

(47) Hong, M. (2006) Solid-State NMR Studies of the Structure and Dynamics of Disordered and Membrane-Bound Peptides and Proteins. *Acc. Chem. Res. 39*, 176–183.

(48) Huster, D., Yao, X. L., and Hong, M. (2002) Membrane Protein Topology Probed by ^{1}H Spin Diffusion from Lipids Using Solid-State NMR Spectroscopy. *J. Am. Chem. Soc. 124*, 874–883.

(49) Kumashiro, K. K., Schmidt-Rohr, K., Murphy, O. J., Ouellette, K. L., Cramer, W. A., and Thompson, L. K. (1998) A novel tool for probing membrane protein structure: Solid-state NMR with proton spin diffusion and X-nucleus detection. *J. Am. Chem. Soc. 120*, 5043–5051.

(50) Gullion, T., and Schaefer, J. (1989) Rotational-echo double-resonance NMR. *J. Magn. Reson. 81*, 196–200.

(51) Jaroniec, C. P., Tounge, B. A., Herzfeld, J., and Griffin, R. G. (2001) Frequency selective heteronuclear dipolar recoupling in rotating solids: Accurate ^{13}C-^{15}N distance measurements in uniformly ^{13}C,^{15}N-labeled peptides. *J. Am. Chem. Soc. 123*, 3507–3519.

(52) Bak, M., Rasmussen, T., and Nielsen, N. C. (2000) SIMPSON: A General Simulation Program for Solid-State NMR Spectroscopy. *J. Magn. Reson. 147*, 296–330.

(53) Prenner, E. J., Lewis, R. N., Neuman, K. C., Gruner, S. M., Kondejewski, L. H., Hodges, R. S., and McElhaney, R. N. (1997) Nonlamellar phases induced by the interaction of gramicidin S with lipid bilayers. A possible relationship to membrane-disrupting activity. *Biochemistry 36*, 7906–7916.

(54) Fried, V. A., and Rothfield, L. I. (1978) Interactions between lipopolysaccharide and phosphatidylethanolamine in molecular monolayers. *Biochim. Biophys. Acta 514*, 69–82.

(55) Nomura, K., Inaba, T., Morigaki, K., Brandenburg, K., Seydel, U., and Kusumoto, S. (2008) Interaction of Lipopolysaccharide and Phospholipid in Mixed Membranes: Solid-State ^{31}P-NMR Spectroscopic and Microscopic Investigations. *Biophys. J. 95*, 1226–1238.

(56) Seelig, J. (1978) ^{31}P nuclear magnetic resonance and the head-group structure of phospholipids in membranes. *Biochim. Biophys. Acta 515*, 105–140.

(57) Su, Y., DeGrado, W. F., and Hong, M. (2010) Orientation, dynamics, and lipid interaction of an antimicrobial arylamide investigated by ^{19}F and ^{31}P solid-state NMR spectroscopy. *J. Am. Chem. Soc. 132*, 9197–9205.

(58) Doherty, T., Waring, A. J., and Hong, M. (2006) Peptide-lipid interactions of the β-hairpin antimicrobial peptide tachyplesin and its linear derivatives from solid-state NMR. *Biochim. Biophys. Acta 1758*, 1285–1291.

(59) Yamaguchi, S., Huster, D., Waring, A., Lehrer, R. I., Tack, B. F., Kearney, W., and Hong, M. (2001) Orientation and Dynamics of an Antimicrobial Peptide in the Lipid Bilayer by Solid-State NMR. *Biophys. J. 81*, 2203–2214.

(60) Buffy, J. J., McCormick, M. J., Wi, S., Waring, A., Lehrer, R. I., and Hong, M. (2004) Solid-State NMR Investigation of the Selective Perturbation of Lipid Bilayers by the Cyclic Antimicrobial Peptide RTD-1. *Biochemistry 43*, 9800–9812.

(61) Aisenbrey, C., Bertani, P., and Bechinger, B. (2010) Solid-state NMR investigations of membrane-associated antimicrobial peptides. *Methods Mol. Biol. 618*, 209–233.

(62) Auger, M. (2009) Structural and Dynamics Studies of Lipids by Solid-State NMR. *Encyclopedia of Magnetic Resonance*, John Wiley & Sons, Inc., New York.

(63) Brandenburg, K., Koch, M. H., and Seydel, U. (1990) Phase diagram of lipid A from *Salmonella minnesota* and *Escherichia coli* rough mutant lipopolysaccharide. *J. Struct. Biol. 105*, 11–21.

(64) Nomura, K., Maeda, M., Sugase, K., and Kusumoto, S. (2010) Lipopolysaccharide induces raft domain expansion in membrane composed of a phospholipid-cholesterol-sphingomyelin ternary system. *Innate Immun.*in press.

(65) Schromm, A. B., Brandenburg, K., Loppnow, H., Zähringer, U., Rietschel, E. T., Carroll, S. F., Koch, M. H., Kusumoto, S., and Seydel, U. (1998) The charge of endotoxin molecules influences their conformation and IL-6-inducing capacity. *J. Immunol. 161*, 5464–5471.

(66) Urbán, E., Bóta, A., and Kocsis, B. (2006) Non-bilayer formation in the DPPE-DPPG vesicle system induced by deep rough mutant of *Salmonella minnesota* R595 lipopolysaccharide. *Colloids Surf., B 48*, 106–111.

(67) Brandenburg, K., Koch, M. H., and Seydel, U. (1998) Biophysical characterisation of lysozyme binding to LPS Re and lipid A. *Eur. J. Biochem. 258*, 686–695.

(68) Seelig, J., MacDonald, P. M., and Scherer, P. G. (1987) Phospholipid head groups as sensors of electric charge in membranes. *Biochemistry 26*, 7535–7541.

(69) deAzevedo, E. R., Saalwachter, K., Pascui, O., de Souza, A. A., Bonagamba, T. J., and Reichert, D. (2008) Intermediate motions as studied by solid-state separated local field NMR experiments. *J. Chem. Phys. 128*, 104505.

(70) Jang, H., Ma, B., Lal, R., and Nussinov, R. (2008) Models of Toxic β-Sheet Channels of Protegrin-1 Suggest a Common Subunit Organization Motif Shared with Toxic Alzheimer β-Amyloid Ion Channels. *Biophys. J. 95*, 4631–4642.

(71) Langham, A. A., Ahmad, A. S., and Kaznessis, Y. N. (2008) On the nature of antimicrobial activity: A model for protegrin-1 pores. *J. Am. Chem. Soc. 130*, 4338–4346.

(72) Zhang, Y., Lu, W., and Hong, M. (2010) The Membrane-Bound Structure and Topology of a Human α-Defensin Indicate a Dimer Pore Mechanism for Membrane Disruption. *Biochemistry 49*, 9770–9782.

(73) Su, Y., Doherty, T., Waring, A. J., Ruchala, P., and Hong, M. (2009) Roles of Arginine and Lysine Residues in the Translocation of a Cell-Penetrating Peptide from ^{13}C, ^{31}P, and ^{19}F Solid-State NMR. *Biochemistry 48*, 4587–4595.

(74) Su, Y., Mani, R., and Hong, M. (2008) Asymmetric insertion of membrane proteins in lipid bilayers by solid-state NMR paramagnetic relaxation enhancement: A cell-penetrating peptide example. *J. Am. Chem. Soc. 130*, 8856–8864.

(75) Su, Y., Waring, A. J., Ruchala, P., and Hong, M. (2010) Membrane-bound dynamic structure of an arginine-rich cell-penetrating peptide, the protein transduction domain of HIV TAT, from solid-state NMR. *Biochemistry 49*, 6009–6020.

(76) Doherty, T., Su, Y., and Hong, M. (2010) High-resolution orientation and depth of insertion of the voltage-sensing S4 helix of a potassium channel in lipid bilayers. *J. Mol. Biol. 401*, 642–652.

(77) Freites, J. A., Tobias, D. J., von Heijne, G., and White, S. H. (2005) Interface connections of a transmembrane voltage sensor. *Proc. Natl. Acad. Sci. U.S.A. 102*, 15059–15064.

(78) Li, S., Su, Y., Luo, W., and Hong, M. (2010) Water-protein interactions of an arginine-rich membrane peptide in lipid bilayers investigated by solid-state nuclear magnetic resonance spectroscopy. *J. Phys. Chem. B 114*, 4063–4069.

(79) Raetz, C. R. (1978) Enzymology, Genetics, and Regulation of Membrane Phospholipid Synthesis in *Escherichia coli*. *Microbiol. Rev. 42*, 614–659.